Vehicle/track interaction and ground propagation of vibrations for tramway tracks in urban areas

De Saedeleer, B., Bilon, S., Datoussaïd, S. and Conti, C. *

April 14, 1998

Abstract

One of the main concerns for a light rail transport system manoeuvring in urban areas is the reduction of the acoustic and vibratory nuisances on the neighbourhood. This paper deals with the generation and propagation of ground vibrations induced by tramways coming up against discontinuities at the wheel/rail interface.

A finite-element vehicle/track interaction model is used together with a ground model using Green's functions to compute the propagation of the vibrations at short distance from the source. The vehicle model is formed by combination of bodies (rigid or flexible, rotating bodies like wheelsets or independent wheels) and interconnection elements (spring-damper elements). A residual formulation has been used to establish the dynamic equations of motion. The identification of urban tramway track parameters has been achieved on some usual Belgian urban tramway tracks.

The validity of the model is discussed using an experimental campaign with tramway vehicles passing on a stepwise discontinuity. A parametric analysis has been achieved, which outlines the role of several parameters on the emitted vibrations, such as tramway velocity, track irregularities, wheel resilience or suspension properties.

1 Introduction

The understanding and the evaluation of the vibrations induced by urban vehicles manoeuvring in the cities is of increasing interest: due to the high density of population in the cities, people concerned by the vibratory comfort are more and more numerous, while the recourse to public transport systems will increase in the future.

The purpose of this paper is to estimate the vibratory levels induced by urban railway vehicles, by means of a model taking into account vehicle, track and ground. Such a complete validated model is useful to evaluate changes in

*Faculté Polytechnique de Mons (FPMs), Service de Mécanique Rationnelle, Dynamique et Vibrations, Boulevard Dolez, 31, B-7000, Mons (Belgium)

both the vehicle and the track design in order to reduce the level of vibrations transmitted to the environment.

Vehicle/Track interaction models are quite common in literature [1], but they rarely include soil propagation. It seems indeed that authors considering the coupling through the soil are all concerned by high speed trains (see e.g. [2, 3, 4, 5]), so that at low speeds, like for urban tramways, the coupling through the soil should not be considered. For that reason, we use the soil model after the Vehicle/Track model, just in order to compute the propagation of the vibrations at distance from the track; it is however already quite challenging to model all the path of vibrations (generation and propagation) of surface tracks.

The present paper takes the following structure. At first, the Vehicle/Track system is studied in Section 2: both the model used (Subsection 2.1) and the parameters experimentally identified for the track (Subsection 2.2) are detailed. Then the Soil system is studied in Section 3: on one hand the ground model (Subsection 3.1) is described, on the other hand the connection between the soil model and the Vehicle/Track model is detailed, and thirdly, the parameters for the ground are experimentally identified (Subsection 3.2). Finally, we validate the whole model by measurements of vibrations on vehicles and in the ground in Section 4, before taking a few conclusions about this study in Section 5.

2 The Vehicle/Track system

2.1 Modeling of the Vehicle/Track system

Several models of Vehicle/Track systems have been studied in literature (see [1] for a review), principally in the field of railway vehicles and freight trains [6, 7], or underground systems [8, 9, 10]; the few papers devoted to urban railway vehicles concern either measurements of vibration levels and comparison with standards [11] or experimental assessment of vibratory protection systems [12, 13]. In the case of urban tramway tracks, we have chosen the following Vehicle/Track interaction model, schematically described at Figure 1.

It consists of a classical 2D-model for the track, so-called a 2-layer model, with rigid sleepers and discretely supported rail. The flexible rail (E, I, A_r, ρ_r) is modelized by a Finite Element approach. Railpads and ballast are characterized by springs and dampers (k_p and d_p for the railpad, k_b and d_b for the ballast). The sleepers have a lumped mass m; models with additional ballast masses (so-called 3-layer model) are less common, and there remains anyway a difficulty in experimentally identifying the corresponding additional parameters. A 3D model of the track is also an unnecessary complex task in this context and requires needless supplementary effort in the track characterization; 3D models are specifically used in order to evaluate stresses in ties or noise emission by wheels.

The modeling of the Vehicle itself is achieved in the formalism based on a residual formulation ([14] describes a specific software - URVA [1] - developed at

[1] URVA means *Urban Railway Vehicle Analysis*.

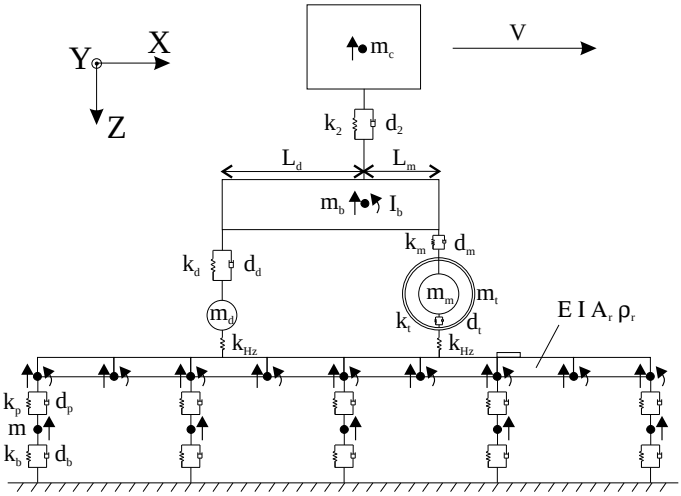

Figure 1: Vehicle/Track model

the FPMs and well adapted to urban railway vehicles design). The vehicle model is formed by combination of bodies (rigid or flexible bodies, rotating bodies like wheelsets or independent wheels) and interconnection elements (spring and damper elements). The track being added under the vehicle, it is necessary to reduce the vehicle behaviour to the degrees of freedom in the same plane than that of the track.

The URVA software has been kept general enough to allow any kind of complex vehicle to be treated, as well as any track type (any spatial distribution and any properties for the rail sections and for the supports). The purpose is not in this paper to introduce an unnecessary complexity in the vehicle and track, but rather to validate the global evaluation of the vibrations induced by the tramway (generation and propagation); both models have therefore been reduced but with the minimum complexity to represent correctly the real dynamic behaviour verified during experimental measurements (see Section 4). The nominal values characterizing the vehicle and track are given in the appendix.

The Vehicle model is composed by a car (m_c), linked to a bogie (m_b, I_b) by means of a secondary suspension (k_2, d_2). The bogie model includes two wheels: a motor wheel (m_m) linked to the bogie at a distance L_m by a primary suspension (k_m, d_m) and a driving wheel (m_d) linked to the bogie at a distance L_d by a primary suspension (k_d, d_d). The motor wheels are equipped by a steel tyre of mass m_t related to the wheel by a resilient material (k_t, d_t).

For the track model, a regular spacing of the sleepers ($L = 0.72m$) has been considered, and a discretization of $N_n = 2$ elements for one sleeper spacing, with a total length of $N = 20$ sleepers have been chosen.

The simulation of the Vehicle/Track system is performed in the time domain, and included nonlinearities (e.g. for contact laws). The contact between wheels

and rail is described by the classical hertzian contact law. A residual formulation has been preferred to write the equations of motion. When combined with the use of a complete iteration matrix [15], this formulation is well adapted to the treatment of stiff differential equations, due to the wheel-rail contacts.

2.2 Experimental identification of the track properties

To quantify the stiffness and damping of urban tracks, we have used the classical receptance concept [16, 17, 18]; the ratio between the vertical displacement response and the vertical excitation force at the top of the rail head is the direct vertical receptance of the track. The identification of the track parameters can be achieved by fitting the numerical direct vertical track receptance to the experimental one (in the frequency domain). With the support of the STIB[2], owner of the tramway network of Brussels (Belgium), such identification has been performed on a typical site.

Experimentally, the excitation of the track is performed either by using an impact hammer or by way of an harmonic source. For the impact, a sledgehammer has been used, while an unbalanced motor acts as harmonic source (see [19] for more details).

Figure 2 compares a series of measurements made on the typical site of Haeren, at several locations on the same track; the receptances given by the impulse hammer (thin lines) are in good agreement with those given by the unbalanced motor (circles). Other measurements coming from other authors [20] at the same place have been added; we note little dispersion between the different trials.

The global shape of the receptance is classical and described in literature [21]: three modes of the track are coming up and were clearly monitored by an experimental modal analysis of the track section. The first mode (at $\approx$ 60 to 80 Hz) corresponds to the motion of the whole track on the ballast resilience k_b. In the second mode (at $\approx$ 350 Hz), the rail and sleeper are in opposite motion through the railpad resilience k_p. The third mode (at $\approx$ 850 Hz) is the pinned-pinned mode of the rail.

On the other hand, the receptance of the track can be computed in the frequency domain, the right term in the receptance matrix being computed from the M, K, C matrices of the track defined by the F.E. model (see Section 2.1) :

$$\frac{x}{F} = \frac{1}{-\omega^2.M + j.\omega.C + K} \tag{1}$$

The identification of the track parameters has been performed by fitting the numerical track receptance to the experimental one, by using a least square minimization criterion, which leads to the following values for the track parameters:

[2]STIB means *Société des Transports Intercommunaux de Bruxelles.*

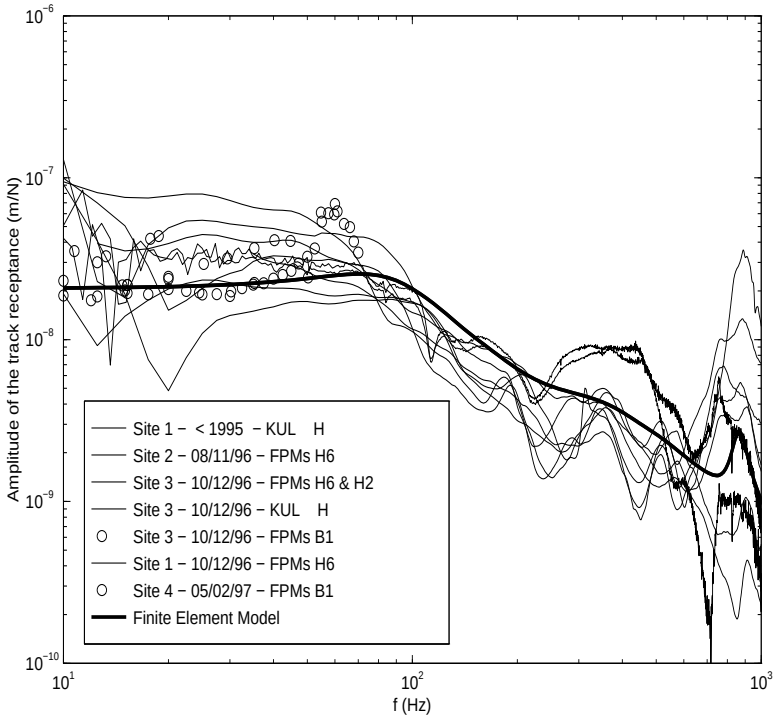

Figure 2: Identification of the track parameters in Haeren 1

$$k_p = 90MN/m, k_b = 25.5MN/m, d_p = 30kNs/m, d_b = 40kNs/m \qquad (2)$$

The static stiffness of the track has also been measured by means of a driving machine [19] which applied a static force on the track, and the measured values of track settlement are in agreement with those obtained from the F.E. model of the track. A global track static stiffness of the order of $60MN/m$ could be deduced for the track of Haeren, while on other sites it could reach up to $350MN/m$.

3 The Soil system

3.1 Modeling of the Soil system

The choice of a model for the ground is governed by the concern for simulating correctly the propagation of the vibrations induced by a tramway running over discontinuities. In that case, the sleepers play a fundamental role: their vertical

vibration on the ground creates 3 types of waves: 2 body waves (the compression waves, called P-waves, and the shear waves, called S-waves), and surface waves (the Rayleigh waves, called R-waves). The faster waves are the P-waves, while the S-waves are a little bit faster than the R-waves (the speeds are in the order $C_p > C_s > C_r$). Those kinds of waves are well described in literature, and analytical expressions are given to compute the speed of those waves, as a function of the Poisson's ratio ν (see e.g. [22]). Authors agree [23, 24] that the Rayleigh wave is predominant energetically speaking for vibrations at distance from the foundation vibrating vertically. So the model should be able to represent the evolution of the R-waves at distance from the sleepers and on the surface of the ground, at the lowest computational cost.

The use of the Green's functions [25] seems the most appropriate, because on one hand it allows arbitrary shaped foundations to be simply studied, and on the other hand it has the advantage of being given on the soil surface, involving calculation only in that plane XY. So the cumulative effect of the sleepers can be taken into account without modeling the soil depth (Z-axis), like it would have been necessary with F.E. methods. In that way, a kind of 3D calculation can be performed with a reduced computation cost: the Vehicle/Track interaction is simulated in the XZ plane, and afterwards the ground displacement pattern in the XY plane is computed from the contribution of all the sleepers.

The Green's functions give the amplitude A and phase ϕ of the Rayleigh wave at the soil surface for each frequency ω, as function of the radius r from the source. Simple analytical expressions have been derived for a point source, then a circle source and finally for a disk source. There exists several precision levels of such functions; the method we used is reduced to the use of approximate Green's functions for a disk source. The displacement w_0 of the disk of radius r_0 laid on a ground of characteristics (G, ν, C_s) submitted to the force of amplitude P at the frequency ω and is given by eq. (3), where a static stiffness K and a reduced frequency a_0 is used.

$$w_0 = \frac{P}{K.(1 + 0.74.i.a_0)} \; with \; K = \frac{4.G.r_0}{1-\nu} \; and \; a_0 = \frac{\omega.r_0}{C_s} \tag{3}$$

The displacement at distance r from that disk can then be deduced through the general formula 4, where the factors of amplitude A and of phase ϕ are specified in Table 1, with a different description of the wave (geometrical damping, phase and speed) in the near field than in the far field (the limit being the radius of the far field, expressed as a fraction of the Rayleigh wavelength $\lambda_r = \frac{2.\pi.C_r}{\omega}$); the value of the parameters are given in eq. (5) for a typical value of ν. Corrections given in eq. (6) may be added to the radius in order to make the point source expressions valid for a disk source: on one hand the phase expressions are adjusted by using an equivalent radius r^*, and on the other hand one adjusts the amplitude expressions by using an equivalent radius $\bar{r}$, especially if one is very near from the disk.

$$w = w_0.A.e^{-i.\phi} \tag{4}$$

	Near field	Limit	Far field
Amplitude	$A = \frac{2.r_0}{\pi.r}$	$r \gtreqless (r_f = \beta.\lambda_r)$	$A = \frac{2.r_0}{\pi.\sqrt{r_f.r}}$
Phase	$\phi = \frac{\omega.r^*}{\gamma.C_r}$	$r^* \gtreqless (r'_f = \beta'.\lambda_r)$	$\phi = \frac{\omega.r^*}{C_r} + \Delta\phi$

Table 1: Approximate Green's functions for a disk

$$for\ \nu = \frac{1}{3}\ we\ have\ \beta \approx 0.3,\ \beta' \approx 1.5,\ \gamma \approx \frac{12}{13}\ and\ \Delta\phi = \frac{\pi}{4} \tag{5}$$

$$r^* = r - \frac{2.r_0}{\pi}\ and\ \bar{r} = r - \frac{(1 - \frac{2}{\pi}).r_0}{(\frac{r}{r_0})^2} \tag{6}$$

Starting from that description of the R-wave generated by a disk, any foundation can be discretized into subdisks, and the vibration of the foundation itself and also at distance from it can be computed. In our case, the sleepers are discretized into subdisks of given size, and they all play the role of source (Figure 3).

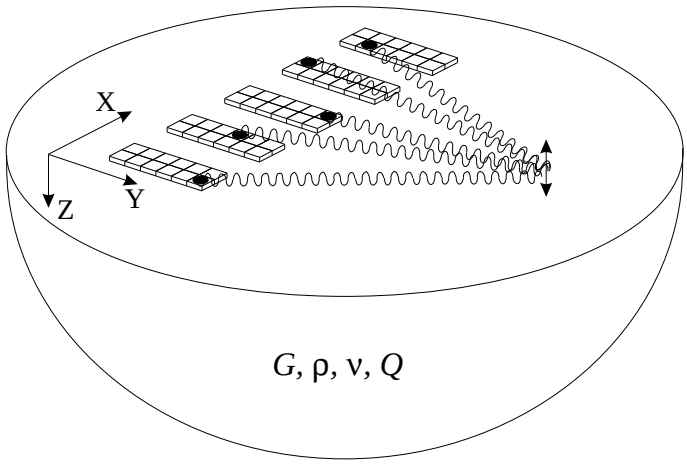

Figure 3: Soil model with the sleepers as vibrating sources

Let's recall that the calculations are made in the frequency domain: the frequency component of the displacement u_0 of one sleeper is obtained by solving

a complex system of equations for each frequency component P of the force acting on the sleeper.

The system to solve is obtained by expressing the influence of each subdisk of the sleeper on the others by using the approximate Green's functions, then by expressing the fact that the sleepers are assumed to be rigid (same displacement for all subdisks u_i), and finally by expressing the consistent fact that the sum of the forces of the subdisks P_i must equals the total force on the sleeper P. For example, these expressions are derived for a discretization of a sleeper into 4 subdisks in eq. (7), (8) and (9), respectively for the complex influence matrix, the rigidity and the consistency.

$$\left\{ \begin{array}{c} u_1 \\ u_2 \\ u_3 \\ u_4 \end{array} \right\} = \left[\begin{array}{cccc} m_{11} & m_{12} & m_{13} & m_{14} \\ m_{21} & m_{22} & m_{23} & m_{24} \\ m_{31} & m_{32} & m_{33} & m_{34} \\ m_{41} & m_{42} & m_{43} & m_{44} \end{array} \right] \cdot \left\{ \begin{array}{c} P_1 \\ P_2 \\ P_3 \\ P_4 \end{array} \right\} \tag{7}$$

$$u_1 = u_2 = u_3 = u_4 = u_0 \tag{8}$$

$$P_1 + P_2 + P_3 + P_4 = P \tag{9}$$

Taking all these relations into account leads to a modified system of equations, as described in eq. (10).

$$\left[\begin{array}{cccc} \frac{1}{m_{11}} & 1 - \frac{m_{12}}{m_{11}} & 1 - \frac{m_{13}}{m_{11}} & 1 - \frac{m_{14}}{m_{11}} \\ \frac{1}{m_{21}} & 1 - \frac{m_{22}}{m_{21}} & 1 - \frac{m_{23}}{m_{21}} & 1 - \frac{m_{24}}{m_{21}} \\ \frac{1}{m_{31}} & 1 - \frac{m_{32}}{m_{31}} & 1 - \frac{m_{33}}{m_{31}} & 1 - \frac{m_{34}}{m_{31}} \\ \frac{1}{m_{41}} & 1 - \frac{m_{42}}{m_{41}} & 1 - \frac{m_{43}}{m_{41}} & 1 - \frac{m_{44}}{m_{41}} \end{array} \right] \cdot \left\{ \begin{array}{c} u_0 \\ P_2 \\ P_3 \\ P_4 \end{array} \right\} = \left\{ \begin{array}{c} P \\ P \\ P \\ P \end{array} \right\} \tag{10}$$

The size of the system to solve corresponds to the number of subdisks for one sleeper. In general, when solving the system, we find a non uniform force distribution between the subdisks. The computation of the influence matrix has been optimized by taking into account the double symmetry of a rectangular sleeper. Once the system has been solved for each sleeper and each frequency component, all the subdisk are then totally charaterized, and they can now be used further to compute the vibrations at distance, with eq. (4) and Table 1. After having determined the displacement spectrum of the ground surface, we can go back to the time domain by an inverse Fourier transform. The evolution of a soil surface area displacement may so be computed and the wave propagation can be viewed by an animation tool automatically linked to the URVA software outputs.

While it is quite clear that the discrete spacing of the sleeper play an important role in the excitation of the Vehicle and in the generation of vibrations in the ground, the relevance of the question of the coupling between sleepers can also be addressed at this stage. As mentioned in the introduction, the coupling through the soil has not to be considered for low speeds, so we did not take neither the interaction between the sleepers into account. Numerically speaking, the fact to take that interaction into account give also rise to much more

large matrices to solve; such a matrix define an impedance function for a whole system of sleepers, like used in [20].

Figure 4 illustrates the propagation of the Rayleigh wave born of the passage of a wheel on a stepwise discontinuity (the x-axis is the track, where we can see the deflection due to the bogie). Quantitative validations of the levels of vibrations in the ground will be given in Section 4.

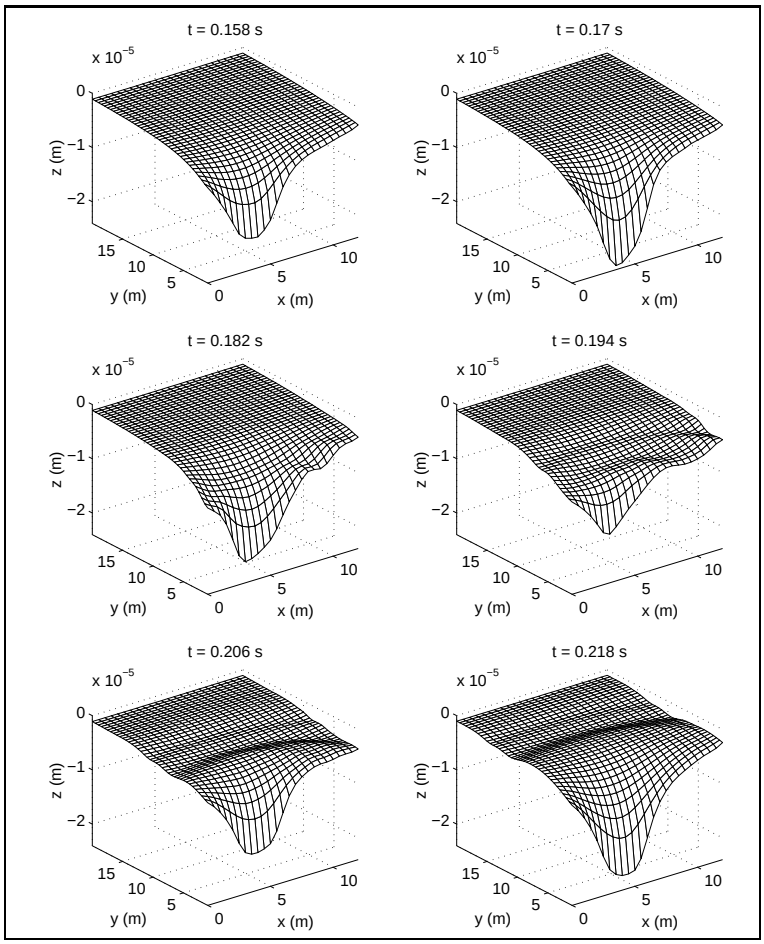

Figure 4: Propagation of the Rayleigh wave from the track

There must be paid attention to the way the sleepers are discretized: there exists a limiting aspect ratio of 4 for the assumption of replacing a subrectangle of sleeper by a subdisk to remain valid [25], and there exists also an overall limit for the subdisk size Δr: the cell must indeed be small enough compared to the wavelength it wants to catch.

The order of magnitude of the required size of the subdisks is well given

in literature: authors all agree on the fact that there must be of the order of 12 cells across one-wavelength of the R-wave to be sure to catch the wave correctly. Authors speaking of Green's functions methods (e.g. [26]) give a limit to the adimensional frequency a_0 of 0.5 which corresponds in fact to the limit of the ground grid size to $\frac{\lambda}{12}$ given for F.E. methods, like in [25], as shown in eq. (11).

$$a_0^{\Delta r} < 0.5 \Leftrightarrow \frac{\omega.\Delta r}{C_s} < 0.5 \Leftrightarrow \frac{2.\pi.\Delta r}{\lambda} < 0.5 \Leftrightarrow \Delta r < \frac{\lambda}{4.\pi} \approx \frac{\lambda}{12} \qquad (11)$$

In order to be sure of the right level of discretization, one has verified that the solution does not depend on the mesh: for the square foundation ($0.33m$ x $0.33m$) configuration used in Section 3.2 to identify the soil properties of Haeren ($C_r = 156m/s$), one has imposed an artificial excitation force made of several discrete frequencies ($1Hz$, $50Hz$, $100Hz$ and $200Hz$). Increasing the level of discretization of the foundation into subdisks (of radius Δr), one checks that the displacement of the foundation was converging. The lowest level of discretization is the level 1 (2x2 elements), and the highest level is the level 5 (10x10 elements). Table 2 gives the ratio $\frac{\lambda_r}{\Delta r}$; we see that there is only one case $\frac{\lambda_r}{\Delta r} < 12$, which is the lowest discretization level coupled with the highest frequency.

		Level of discretization				
		1	2	3	4	5
$f\ (Hz)$	$\lambda_r\ (m)$	2x2	4x4	6x6	8x8	10x10
1	156	1676	3351	5027	6703	8379
50	3.12	34	67	101	134	168
100	1.56	17	34	50	67	84
200	0.78	**8**	17	25	34	42

Table 2: Ratios $\frac{\lambda_r}{\Delta r}$ for several frequencies and discretization levels

If we consider Figure 5, where the relative error has been plotted, we see that the error decreases as the excitation frequency decreases, and decreases also as the level of discretization increases.

The case $\frac{\lambda_r}{\Delta r} < 12$ leads to an error higher than 11%, while in all the other cases the error is less than 5%. From Figure 5 and Table 2, we deduce that the rule of $\frac{\lambda}{12}$ discretization level leads to small errors (less than 5%), but that higher frequencies in the excitation would then require higher level discretization (the smallest wavelength to catch is $\lambda_{min} = \frac{C_r}{f_{max}}$, with f_{max} being the highest frequency we want to account for in the computation).

The URVA software automatically advises the user for the right level of discretization, according to the frequency range and the type of soil considered.

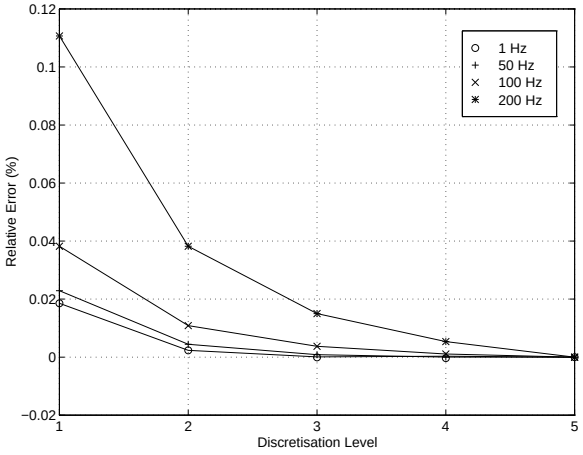

Figure 5: Required level of discretization

They are two significant restrictions to the use of these Green's functions.

On one hand the basic formulation (eq. (4) with Table 1) takes only the geometrical damping into account, but the material damping isn't included. A brief review of literature clearly expresses the dearth of information on the energy dissipation aspects for a soil. It is generally agreed that the decay in amplitude due to the damping effects can be represented in the form $A(r) = A_0.e^{-\alpha.r}$. The controversial issue is the frequency dependence of the absorption coefficient α. While Barkan [27] gives a frequency-independent coefficient α, authors more and more agree on the fact that it must be frequency-dependent [24, 28]. It is now generally assumed that α is linearly dependent on frequency by the formula $\alpha = \frac{\pi.\eta}{c}.f$, where η is the (constant) *loss factor*, and c is the appropriate wave speed. Equivalent expressions use a *quality factor* Q, which is in fact the inverse of the loss factor η. So the Green's functions have been modified to account for this type of material damping.

On the other hand the basic formulation used for the Green's functions (eq. (4) with Table 1) is valid only for an homogeneous halfspace; similar expressions could however be obtained by the use of a more general method, like the Boundary Element Method (BEM). To take the layering of the ground into account, one should at least be able to do seismic determination of the speeds in each layer; what has been considered in our case as an unnecessary complexity, seeing that it is often difficult to know precisely the structure of the underground in the cities, or even to measure it.

There must also be paid attention on the way the soil model is connected to the Vehicle/Track model: the time simulation of the Vehicle/Track system gives indeed temporal evolutions of degrees of freedom, while the soil model described by the Green's functions require a spectral description of the forces acting on the foundations resting on the ground. The link can be easily done

by taking as input for the soil the Fourier transform of the forces acting on the soil, represented by the force in the ballast element ($F_{soil} = K_b.x_{sl} + D_b.\dot{x}_{sl}$); after having calculated the propagation by Green's functions, one can return to the time domain by an inverse Fourier transform.

3.2 Experimental identification of the soil properties

After having described the soil model, the relevant parameters (G, ν and Q) have to be identified experimentally.

A semi-infinite space is totally determined by its density ρ and by its wave speeds C_p, C_s, C_r. The ratio $\chi = \frac{C_s}{C_p}$ yields the Poisson's ratio ν of the soil by eq. (12) and the Rayleigh wave velocity C_r by solving eq. (13) - see e.g. [22] for the theoretical developments). The shear modulus G may then be deduced once one knows the density ρ of the soil by eq. (14).

$$\nu = \frac{1 - 2.\chi^2}{2.(1 - \chi^2)} \tag{12}$$

$$\kappa^6 - 8.\kappa^4 + (24 - 16.\chi^2).\kappa^2 + 16.(\chi^2 - 1) = 0 \; with \; \kappa^2 = \frac{C_r}{C_s} \tag{13}$$

$$G = \rho.C_s^2 \tag{14}$$

The classical way of experimentally identifying the Poisson's ratio ν is to measure at least two of the three wave speeds [29]. The experimental procedure for soil measurements has been first validated on a site where a lot of expert soil experiments were conducted [30, 31]; soil experiments were then conducted on the track network of Haeren. Triaxial accelerometers distant from 0.5, 3, 5, 10, 15, 20 and $30m$ from the source measured the soil acceleration. The excitation was produced by a falling weight device (Figure 6), giving rise to the three types of waves; the energy distribution between the waves is the one that one can expect from vertically vibrating foundations (see Section 3.1 for the details), like the sleepers. A weight of $50kg$ falls from $1m$ height on a square foundation $0.33m$ x $0.33m$.

The normalized vertical accelerations (filtered between $5Hz$ and $500Hz$) at the several stations are displayed at Figure 7. Making a regression on the first arrivals of the several stations gives a value of $305m/s$ for the highest wave speed, C_p. The difficulty for the identification of the first arrivals is that the P-wave is less energetic than the other waves for that type of excitation, and that it may be difficult to distinguish the beginning of the perturbation from the ambient noise level.

The identification of the speed of the Rayleigh waves C_r on the basis of Figure 7 is much less easy, because one has difficulties to isolate one Rayleigh wave, as R-waves arrive in last position and are not well developed in the vicinity of the impact; perturbations of R-waves may also occur, due to reflections of faster waves on lower layers in the ground. Without using more specific methods for soil identification, like in [30, 31], one can however deduce an estimated value

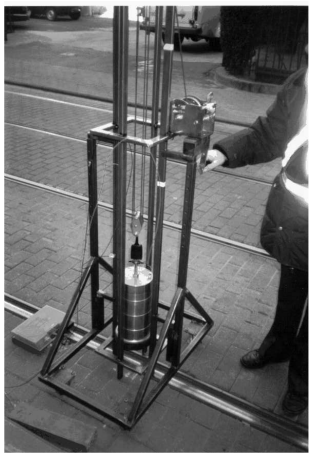

Figure 6: Falling weight device for an impact excitation

for C_r by monitoring the orbit of particle motions at the ground surface, like done e.g. in [28], in order to be sure that the wave taken for the speed identification is well that of Rayleigh. As example, Figure 8 shows the orbit of particle motion at 5m of the vertical impact. We can see a counterclockwise elliptic motion, which is peculiar to the Rayleigh wave; this behaviour is recognized also for other stations, allowing to identify the zones of Rayleigh behaviour in Figure 7, and hence to be sure of that the wave speed identified at $C_r = 156m/s$ corresponds to the Rayleigh wave.

From $C_p = 305m/s$ and $C_r = 156m/s$, we can deduce a value of 0.28 for the Poisson's ratio ν, and of $169m/s$ for C_s, which is a bit faster wave than the R-wave. The value of the shear modulus $G = 5.7E7N/m^2$ can then be deduced, as soon as the density of the soil ρ was identified to be of the order of $2000kg/m^3$.

The identification of the quality factor Q characterizing the soil damping behaviour (see Section 3.1) can be achieved by making the ratio between the spectra of 2 measurement stations spatially apart [29]; a regression on the semilogarithmic values makes appear the quality factor Q as linked to the slope of the curve. A value of $Q = 12.5$ has been identified on the site of Haeren.

An intermediate verification of that damping modeling can be made by simulating the displacement of the soil surface due to the vertical impact given experimentally by means of the falling-weight device. We used the model based on the simple Green's functions with the parameters of the experiment (square foundation of $0.33m$ x $0.33m$, input force measured by means of an accelerometer fixed on the falling weight). The maximum of the displacement of the soil surface at each station is plotted at Figure 9, where the measurements are compared to the results of the model with and without material damping. We see that the material damping has to be introduced, and that the constant-Q

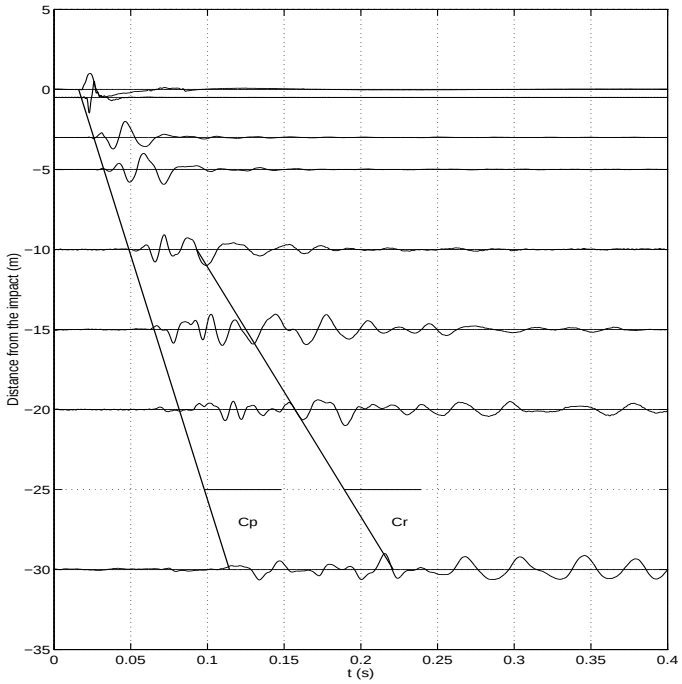

Figure 7: Evolution of the normalized vertical acceleration on the ground

formulation is quite satisfactory. A better estimation of the general damping law $A(r) = A_0.e^{-\alpha.r}$ is nevertheless about to be done at the same place with an harmonic excitation (electromagnetic shaker), in order to assess the assumption of linearly dependence of α with the frequency.

Let's note that a lot of deeper analyses were conducted on the soil experiments, but that this it is not the aim of the present paper to discuss soil experiments into details; so we give here only the 4 most important conclusions we have noted: impacts and measurements in all axis were very well repeatable; other types of impact (radial and transverse) were used to excite more specifically one given type of wave, and they all confirm the identified wave speeds; levels in the soil seemed to be linearly linked to the level of the excitation (we used several mass drop heights); and finally the polynomial fitting law $y = b.r^a$ for the material damping, like suggested by few authors [32], gave inaccurate results near the source.

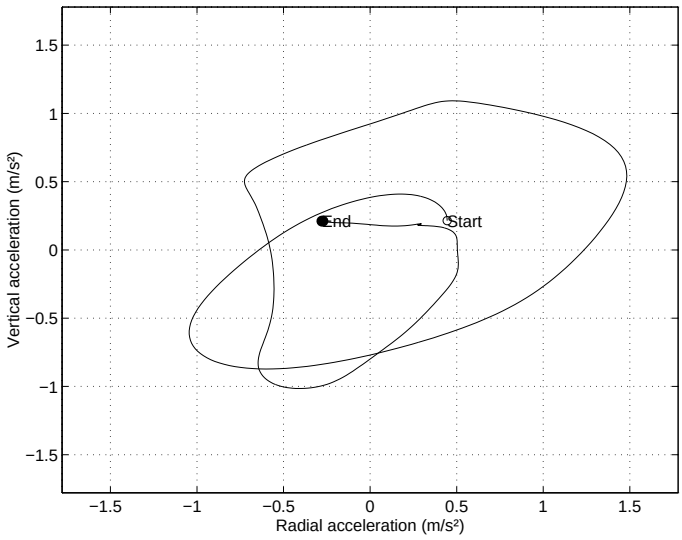

Figure 8: Orbit of particle motion at 5m of the vertical impact

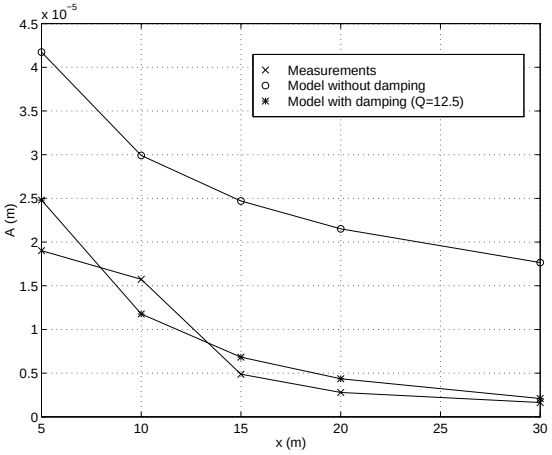

Figure 9: Validation of the material damping formulation

4 Validation of the complete Vehicle/Track/Soil model

The tramway site of Haeren having been completely identified regarding the track and the soil properties, an experimental campaign was undertaken with tramways in order to validate the complete Vehicle/Track/Soil model in a representative situation of the vibration generation and propagation.

The choice of a representative excitation has been made by taking into account the fact that the most important source of vibrations are crossings, switch gears and rail discontinuities like rail joints (see e.g. conclusions of [12]); a reference case has been defined as a stepwise discontinuity of $1mm$ height by $5mm$ length. One could also think to a change of stiffness in the track as excitation (like in [33]), but that was experimentally denied in our specific case (with experiments conducted via the driving machine); for a real change of track stiffness to be considered, there should be a real significant change in the track properties.

The experimental vehicle is the new tram T2000 LRV evolving now in Brussels (Figure 10). It is a modern multi-cars tramway which uses advanced technology like independent rotating wheels [34, 35] and low floor design.

Figure 10: The tram T2000 of Brussels (Belgium)

The effect of changes in the tramway design can be considered in order to reduce the vibrations emitted. Resilient wheels are described in literature as leading to a global improvement both for the vehicle and for the track care (with expected lower vibrations emitted), because of their ability to reduce the dynamic wheel/rail force at vertical track irregularities [36, 37, 38]; resilient wheels were even considered able to reduce the noise emitted [37, 39].

Several prototypes of tramway were equipped with resilient wheels; the

results described in this paper corresponds to a value of wheel stiffness of $k_t = 13MN/m$ for the resilient wheels, while a value of $k_t = 145MN/m$ was considered for the nominal wheels.

For the model of the vehicle, we only consider the leading bogie of the tram (Figure 1), the behaviour of the other wheels being similar. The nominal value of the parameters used for the vehicle, track and ground are listed in the appendix; the track and soil parameters are those identified respectively in Section 2.2 and 3.2. The size of the sleepers is $0.24m$ x $2.6m$ x $0.14m$ (width x length x height).

The validity of the Vehicle/Track model can be assessed by plotting the evolution of a characteristic quantity when the tramway is running on the stepwise discontinuity, as for example the vertical acceleration of the motor (fixed on the wheel). Figure 11 shows the comparison between measurements and modeling, for the 2 types of tramways and at different velocities (the 4 big tics correspond to the contact phases of the circular wheel with the stepwise discontinuity: encounter, start of running-on, end of running-on, departure). We see that the model correctly predicts both the level and shape of the evolution in all the cases; higher frequencies perturbation may come from a wheel flat, as often established during experiments.

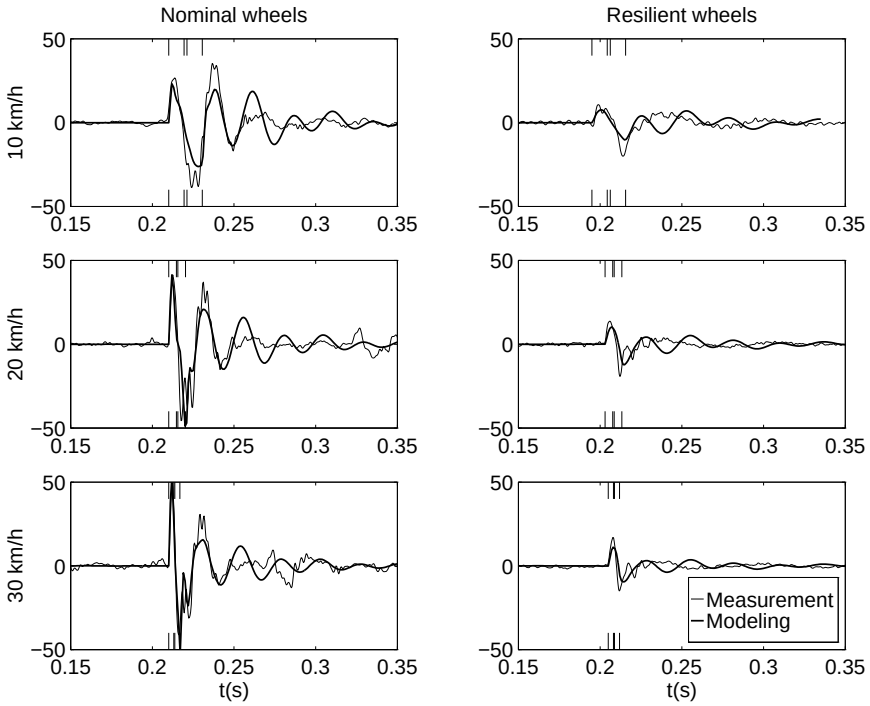

Figure 11: Vertical acceleration of the motor

The validity of the Soil model can be assessed by plotting the evolution of the soil surface velocity at given points. Figure 12 illustrates the comparison between measurements and modeling of the soil vertical velocity at $2m$ of the track, always for both tramways at different velocities. In order to obtain soil surface velocities, the accelerometric measurements have been integrated while the model predictions of displacements have been derived. We see that there is a fairly good agreement on the soil vibration predictions, not only in the levels, but even also in the shape.

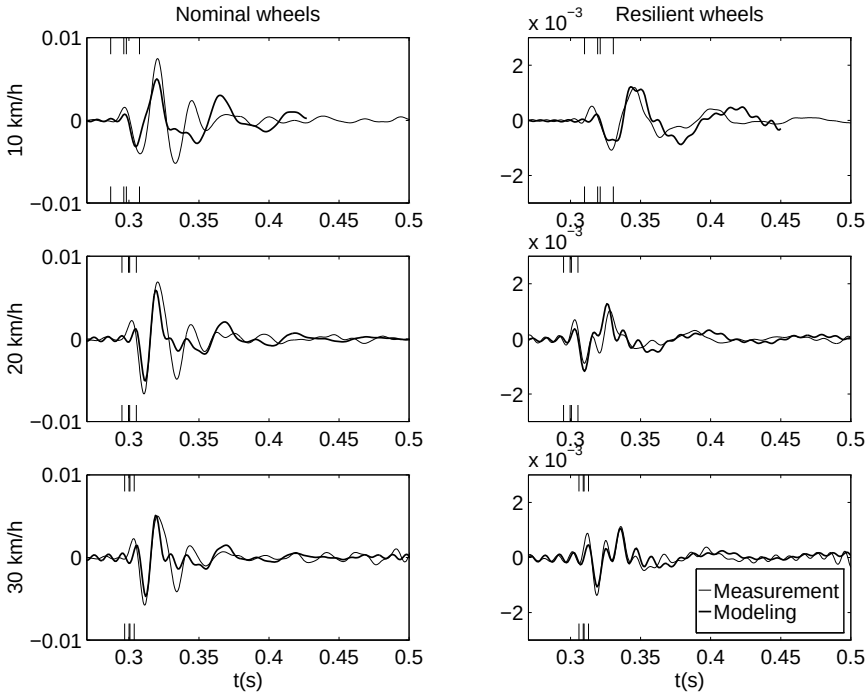

Figure 12: Vertical velocity of the ground at 2m from the track

A second prediction, a little bit further from the track validate also the damping model adopted for the ground (Figure 13). More significant differences may occur due to a more and more perturbed signal as long as the distance from the track increases; a slight time-shift may also occur if wave speeds are not exactly determined, but is not very troublesome.

The results of Figures 11 to 13 may directly be used as an elementary parametric study: we see the effect of the resilience of the wheel, of the tramway speed, and of the distance from the track. Making the wheels more resilient decreases the level of acceleration on the motor and bogie, and reduces the vibrations into the ground.

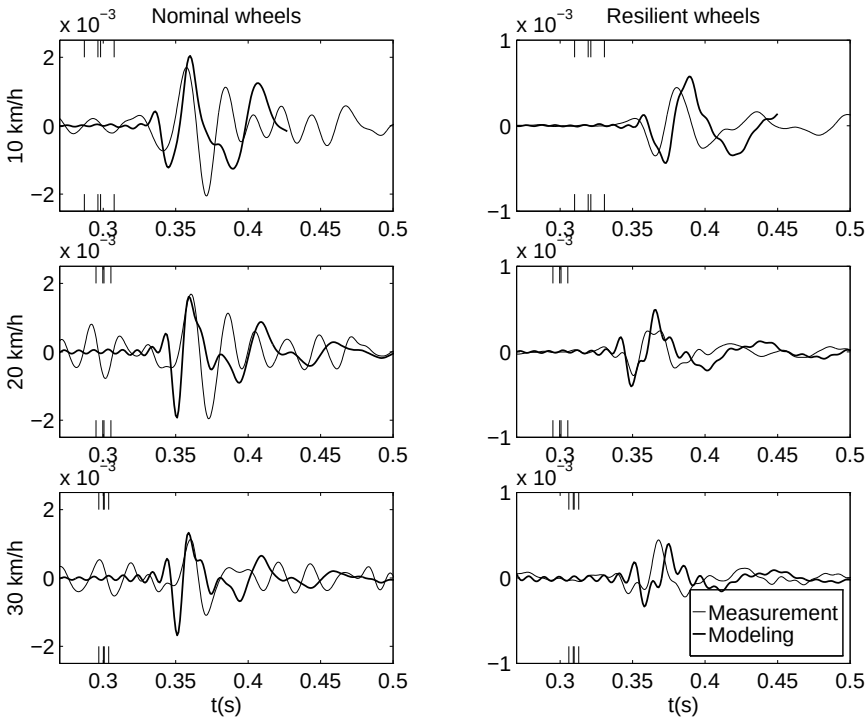

Figure 13: Vertical velocity of the ground at 8m from the track

5 Conclusions

This paper contributes to have a global view on the vibrations induced by tramways running against discontinuities at the wheel/rail interface: it deals with the generation but also with the propagation of the vibrations into the ground.

The URVA software which was dedicated to urban railway vehicles has now been equipped with a track and ground model. They consist in a finite-element vehicle/track interaction model to compute the generation, together with an approximate Green's functions model for the soil to compute the propagation of the vibrations.

All the inputs of the models (urban tramway track parameters and soil parameters) have been experimentally identified on the typical tramway site of Haeren (Belgium).

The complete Vehicle/Track/Soil model has then been validated by means on an experimental campaign with tramway vehicles passing on a stepwise discontinuity. The validation has been done on both vehicle and ground sides, on the basis of criteria such as motor acceleration and ground velocities, for several

level of wheel resilience, several tramway speeds and several distances from the track. The overall good agreement (level and shapes) between the predicted quantities and the measurements shows that the Vehicle/Track/Soil model proposed is adapted to predict the vibration levels both in the vehicle and in the ground.

Some conclusions could already be drawn from the results obtained during the validation phase, as for example that making the wheels more resilient reduces the level of acceleration on the motor and bogie, and reduces also the vibrations into the ground. Deeper analyses may be conducted e.g. in order to investigate frequency contents of the vibrations.

Further improvements of URVA should include experimental characterization of the transmissibility for more complex site situations (with pavements in the city); some transmissibilities have moreover already been measured at typical locations in Brussels. Deeper validation is expected from measuring the contact force at the wheel/rail interface by means of strain gauges. A better estimation of the general damping law $A(r) = A_0.e^{-\alpha.r}$ is expected from an harmonic excitation (electromagnetic shaker).

6 Acknowledgements

We are grateful to the "Région Wallonne" (RW) of Belgium for supporting the research, to Bombardier Eurorail (BN) for having carried out the changes in the design of the trams, and to the "Société des Transports Intercommunaux de Bruxelles" (STIB) for having given noticeable help in measurement campaigns on their tramway network.

References

[1] Knothe, L. and Grassie, S.L., "Modelling of Railway Track and Vehicle/Track Interaction at High Frequencies", VSD, 22 (1993), 209-262, Swets and Zeitlinger BV, Lisse, Netherlands

[2] Auersch, L., "Zur Parametererregung des Rad-Schiene-Systems: Berechnung der Fahrzeug-Fahrweg-Untergrund-Dynamik und experimentelle Verifikation am Hochgeschwindigkeitszug Intercity Experimental", Ing. - Arch. 60 (1990), pp. 141-156

[3] Rohrmann-Baumgart, R.G., Rücker, W., "Dynamische Bodenkennwerte für Scotteroberbau aus Halbraumtheorie", ETR 36 (1987), pp. 587-591

[4] Rücker, W., "Dynamic Interaction of a Railroad-Bed with the Subsoil", Soil Dynamics & Earthquake Engineering Conference, Southampton, July 1982, pp. 435-448

[5] Sarfeld, W., Savidis, S.A., Schuppe, R. and Klapperich, H., "Three-dimensional dynamic interaction of ties", Xth ICSMFE (Internationale Baugrundtagung), Stockholm, 1981, pp. 287-292

[6] Dawn, T.M. and Stanworth, C.G., "Ground vibration from passing trains", Journal of Sound and Vibrations, 1979, Vol. 66, No. 3, 355-362

[7] Netter, H., Schupp, G., Rulka, W. and Schroeder, K., "New Aspects of Contact Modelling and Validation Within Multibody System Simulation of Railway Vehicles", in: "The Dynamics of Vehicles on Roads and on Tracks", Proceedings of the 15th IAVSD-Symposium Budapest 1997, to appear.

[8] Kurzweil, L.G., "Ground-Borne Noise & Vibration from Underground Rail System", Journal of Sound & Vibration, 66(3), 363-370, 1979

[9] Heckl, M., "Suppressing vibrations from Metro Trains", Railway Gazette International, January 1987, 40-42

[10] Balendra, T., Koh, G.C., Ho, Y.C., "Dynamic Response of building due to trains in underground tunnels", Earthquake Eng. and Struct. Dynamics, Vol. 20, 1991, 275-291

[11] Martin, D.J., "Low Frequency Traffic Noise & Building Vibration", Techn. Rep., Transport & Road Research Laboratory, Crowthorne, Berkshire, 1978

[12] Clement, H., "Les voies ferrées de métro et la protection de l'environnement dans un milieu très urbanisé", Proc. of workshop of 6th Dec. 1994 in Paris, organised by the C.S.T.B. and called "Les vibrations dans les bâtiments dues aux transports ferroviaires"

[13] Colnat, J., "Problèmes de bruit et vibrations dus aux transports ferroviaires en milieu urbain: dispositifs de protection", Revue Travaux, septembre 1981

[14] Datoussaïd, S., Verlinden, O., Wenderloot, L. and Conti, C., "Computer-aided dynamics of urban railway vehicles", Proceedings of the International Workshop on Computer Simulation of Rail Vehicle Dynamics, 23-24 juin 1997, Manchester, pp. 1-14

[15] Verlinden, O., Dehombreux, P. and Conti, C., "An optimized residual formulation of multibody systems", First Joint Conference of International Simulation Societies, Zurich (Switzerland), pp 307-311, Augustus 1994

[16] Vincent, N. and Thompson, D.J., "Track Dynamic Behaviour at High Frequencies - Part 2: Experimental Results and Comparisons with Theory", VSD Supplement 24 (1995) pp. 100-114

[17] Grassie, S.L., Gregory, R.W., Harrison, D. and Johnson, K.L., "The dynamic response of railway track to high frequency vertical excitation", IMechE, JMES, 1982, Vol. 24, No. 2, 77-90

[18] Grassie, S.L., and Cox, S.J., "The dynamic response of railway track with unsupported sleepers", Proceedings of IMechE, Part D, 1985, Vol. 199, No. 2, 123-135

[19] De Saedeleer, B., Bilon, S., Datoussaïd, S. and Conti, C., "Vibrations induced by urban railway vehicles - Modeling of the Vehicle/Track system", Proceedings of the "Transport et Environnement" study days of the BSMEE (Belgian Society of Mechanical and Environmental Engineering), held in Mons (Belgium), 28-29 May 1998

[20] Van den Broeck, P., "Trillingshinder in een bebouwde omgeving ten gevolge van treinverkeer", Periode: februari 1994 - maart 1995 - Verslag maart 1995

[21] Ripke, B., and Knothe, K., "Die unendlich lange Schiene auf diskreten Schwellen bei harmonisher Einzellasterregung", VDI Fortschritt-Bericht, Reihe 11, Nr. 155, Düsseldorf, 1991

[22] Richart, F.E., Jr, Hall, T.R., Jr and Woods, E.D., "Vibrations of Soils and Foundations", Englewood Cliffs, New Jersey: Prentice-Hall, Inc

[23] Miller, G.F. and Pursey, H., "On the partition of energy between elastic waves in a semi-infinite solid", Proc. of the Royal Society, London, Vol. 233, 55-69

[24] Gutowski, T.G. and Dym, C.L., "Propagation of Ground Vibration: a review", Journal of Sound and Vibrations, 1976, Vol. 49, No. 2, 179-193

[25] Meek, J.W. and Wolf, J.P., "Approximate Green's function for surface foundations", Journal of Geotechnical Engineering, ASCE 119 (1993): 1499-1514

[26] Kuhlemeyer, R.L. and Lysmer, J., "Finite Element Method Accuracy for Wave Propagation Problems", Journal of the Soil Mechanics & Foundation Division, ASCE, Vol. 99, No. SM5, Proc. Paper 9703, May 1973, pp. 421-427

[27] Barkan, D.D., "Dynamics of Bases and Foundations", New York, McGraw-Hill Book Company, Inc, 1962

[28] Taniguchi, E. and Sawada, K., "Attenuation with distance of traffic-induced vibrations", Soils Found. J. Jpn. Soc. Soil Mech. Found. Engrg, 19(2), 15-28, 1979

[29] Jongmans, D., "The application of seismic methods for dynamic characterization of soils in earthquake engineering", Bulletin of the International Association of Engineering Geology, 46, pp.63-69

[30] Jongmans, D. and Demanet, D., "The importance of surface waves in vibration study and the use of Rayleigh waves for determining the dynamic characteristics of soils", Engineering Geology, 34, 105-113

[31] Jongmans, D., Demanet, D., and Horrent, C., "Transmission des ondes de vibration dues aux chantiers de construction et interaction sol-structure", CSTC - ULg - KUL - Convention IRSIA CI 1/4 - 7672/091 - Biennale 1991-1993 - Novembre 1993

[32] Le Houédec, D. and Picard, J., "Validation in situ de la théorie des barrières de discontinuités dans le sol", Ministère de l'Environnement, Contrat SRETIE No. 89218, Rapport final, 1993

[33] Fröhling, R.D., "Low Frequency Dynamic Vehicle/Track Interaction: Modelling and Simulation", Proceedings of the 15th IAVSD-Symposium Budapest 1997

[34] Datoussaïd S., Verlinden O. Conti C. and Dehombreux P., "Méthodologie d'analyse dynamique latérale des véhicules ferroviaires urbains", International Symposium on Technological Innovation in Guided Transports (Lille), vol.2, pp 747-755, September 1993

[35] Fisette P. and Samin J.C., "Lateral Dynamics of Light Railway Vehicle with independent wheels", 12th IAVSD Symposium on Dynamics of Vehicles on Roads and Tracks, pp 157-171, Augustus 1991

[36] Björk, J., "Dynamic loading at rail joints - effect of resilient wheels", Railway Gazette, June 5, 1970, 430-434

[37] Cavell, B.G., "Resilient wheels of SAB design applied to mainline locomotives of high power", Rail Engineering International, 1974, 2-8

[38] Jenkins, H.H., Stephenson, J.E., Clayton, G.A., Morland, G.W. and Lyon, D., "The Effect of Track and Vehicle Parameters on Wheel/Rail Vertical Dynamic Forces", Railway Eng. J., Jan. 1974, Vol. 3, No. 1, 2-16

[39] Hemelrijk, R., "Het effekt van wieldempers op de geluidemissie van treinen (The effect of wheel dampers on the sound emission of trains)", Proceedings of the N.A.G. (Dutch Acoustical Society), 67, 27-37, 1983

Appendix : List of symbols

Symbol	Meaning	Nominal value	Units
A	amplitude of the R-wave displacement	-	m
a_0	reduced frequency	$\frac{\omega.r_0}{C_s}$	1
A_0	displacement at the source	-	m
A_r	section of the rail	0.00638	m^2
$A(r)$	displacement at distance	$A_0.e^{-\alpha.r}$	m
C_p	speed of the compression wave	305	m/s

continued on next page

continued from previous page

Symbol	Meaning	Nominal value	Units
C_r	speed of the Rayleigh wave	156	m/s
C_s	speed of the shear wave	169	m/s
d_2	damping of the secondary suspension	56250	Ns/m
d_b	ballast damping	40E3	Ns/m
d_d	driving wheel suspension damping	6E3	Ns/m
d_m	motor wheel suspension damping	18E3	Ns/m
d_p	railpad damping	30E3	Ns/m
d_t	resilient tyre suspension damping	3E3	Ns/m
E	Young's modulus of rail material	210E9	N/m^2
f	frequency of the excitation	-	Hz
f_{max}	highest frequency of excitation	-	Hz
F_{soil}	force acting on the sleeper soil surface	-	N
G	shear modulus of the soil medium	5.7E7	N/m^2
I	rotational inertia of the rail	1.9878E-5	m^4
I_b	rotational inertia of the bogie	300	$kg.m^2$
K	static stiffness of a disk source	$\frac{4.G.r_0}{1-\nu}$	N/m
k_2	stiffness of the secondary suspension	96E4	N/m
k_b	ballast stiffness	2.55E7	N/m
k_d	driving wheel suspension stiffness	5.876E6	N/m
k_{Hz}	linearized Hertzian contact stiffness	1E9	N/m
k_m	motor wheel suspension stiffness	4.408E7	N/m
k_p	railpad stiffness	9E7	N/m
k_t	resilient tyre suspension stiffness	145E6	N/m
L	sleeper spacing	0.72	m
L_d	distance driving wheel - bogie c.g.	-1.13	m
L_m	distance motor wheel - bogie c.g.	0.57	m
m	mass of one half sleeper	45.42	kg
m_b	mass of the bogie	1800	kg
m_c	mass of the car	7580	kg
m_d	mass of the driving wheel	160	kg
m_{ij}	complex influence matrix element	-	m/N
m_m	mass of the motor wheel	1890	kg
m_t	mass of the resilient tyre	80	kg
N	number of sleepers	20	1
N_n	discretization of a sleeper spacing	2	1
P	amplitude of the excitation force	-	N
P_i	force acting on a subdisk	-	N
Q	quality factor for soil material damping	$\frac{1}{\eta} = 12.5$	1
r	distance from the source	-	m
$\bar{r}$	equivalent radius for correction in A	$r - \frac{(1-\frac{2}{\pi}).r_0}{(\frac{r}{r_0})^2}$	m

continued on next page

continued from previous page			
Symbol	Meaning	Nominal value	Units
r^*	equivalent radius for correction in ϕ	$r - \frac{2.r_0}{\pi}$	m
r_0	radius of a disk source	-	m
r_f	radius of the far field for A	$\beta.\lambda_r$	m
r'_f	radius of the far field for ϕ	$\beta'.\lambda_r$	m
u_0	displacement of one sleeper	-	m
u_i	displacement of a sleeper subdisk	-	m
w	displacement at distance	$w_0.A.e^{-i.\phi}$	m
w_0	displacement of a disk source	$\frac{P}{K.(1+0.74.i.a_0)}$	m
x_{sl}	displacement of a sleeper	-	m
α	coefficient for soil material damping	-	$1/m$
β	adimensional ratio $\frac{r_f}{\lambda_r}$	0.3	1
β'	adimensional ratio $\frac{r'_f}{\lambda_r}$	1.5	1
γ	correction of speed in the near field	$\frac{12}{13}$	1
Δr	radius of a subdisk	-	m
$\Delta\phi$	correction of phase in the far field	$\frac{\pi}{4}$	rad
η	loss factor for soil material damping	0.08	1
κ	ratio of the R-wave and S-wave speeds	$\frac{C_r}{C_s} = 0.9231$	1
λ_{min}	lowest Rayleigh wavelength	$\frac{C_r}{f_{max}}$	m
λ_r	Rayleigh wavelength	$\frac{2.\pi.C_r}{\omega}$	m
ν	Poisson's ratio of the soil medium	0.28	1
ρ	density of the soil medium	2000	kg/m^3
ρ_r	density of rail material	7850	kg/m^3
ϕ	phase of the R-wave displacement	-	rad
χ	ratio of the S-wave and P-wave speeds	$\frac{C_s}{C_p} = 0.5541$	1
ω	angular velocity of the excitation	-	rad/s

Table 3: Meaning and nominal values of the symbols